The Dynamic Balance of Internal Waves

C. HENRY MCCOMAS[1]

Woods Hole Oceanographic Institution, Woods Hole, MA 02543

PETER MÜLLER[2]

Harvard University, Cambridge, MA 02139

(Manuscript received 16 January 1981, in final form 6 April 1981)

ABSTRACT

For oceanic internal waves with vertical scales larger than 1 m the evolution of the spectrum is adequately described by weak-interaction theory. Based on simple physical arguments, a model for internal-wave energy dissipation predicts dissipation as weak over the same scales, for reasonable values of the total dissipation. Assuming dissipation at small scales, such as in our proposed model, and generation at large scales, a consistent dynamic balance with a constant downscale energy flux under nonlocal nonlinear interactions reproduces the observed spectral dependencies. A small-scale break point at which the total shear reaches a given value, and beyond which dissipation is important, is determined by the level and bandwidth of the energy-containing waves.

1. Introduction

When Garrett and Munk (1972a, 1975), henceforth GM, were able to distill diverse observations into a consistent and highly reliable model of the internal wave spectrum, the search for the mechanism(s) controlling the spectral levels and dependencies began. The first efforts centered on numerical evaluations of weak nonlinear resonant interactions (Olbers, 1976; McComas and Bretherton, 1977, hereafter MB). Olbers showed that energy could be transferred from large vertical scales to fill out the rest of the spectrum, and he determined the basic time scales for that process. MB looked at the dynamics of the smaller scale waves and discovered three mechanisms dominating the transfers. The first, termed elastic scattering, brought the upgoing and downgoing waves to equal intensities at the higher frequencies, having no effect at near inertial waves. This "vertical symmetry" is an established feature of the deep-ocean spectrum (e.g., Leaman and Sanford, 1975; Müller *et al.*, 1978). The second mechanism, called parametric subharmonic instability, transferred energy to smaller scale waves with half the frequency of the unstable wave. This process was most effective at low frequencies, transferring energy into the small-scale inertial band. The third mechanism, induced diffusion, acted as wave-action diffusion in wavenumber space. Most of the supra-inertial spectrum was dominated by this mechanism, and the GM models were close to equilibrium for this interaction.

To demonstrate the nature and dominance of the elastic-scattering and induced-diffusion mechanisms, McComas (1977) calculated transfers in various perturbed spectra. Although a coding error led to an overestimate of the efficiency of the elastic-scattering process (recalculated by McComas and Müller, 1981, hereafter MM), both mechanisms gave short relaxation times at the smallest scales. In particular, for a 10% spike, the induced-diffusion mechanism produced time scales that were shorter than a period over most of the spectrum, violating the basic assumption of weak interaction.

Such difficulties, discussed by Holloway (1980), have initiated attempts to describe strong off-resonant interactions. However, these efforts, which are much more involved than the already complicated weak theory, have yet to yield results. Further, MM have argued that as long as dissipation is weak, the weak theory adequately describes the transfers in the resulting smooth spectra down to scales of about 1 m.

Hopes to verify observationally the dominating mechanisms using bispectral techniques were dashed when McComas and Briscoe (1980) computed some theoretical bispectra and found the technique statistically inconclusive for any reasonable experiment.

The study of weak nonlinear interactions has been accompanied by various attempts to combine the nonlinear results with ideas about generation and

[1] Presently self-employed.

[2] On leave of absence from the University of Hamburg.

0022-3670/81/070970-17$08.25

dissipation into a complete dynamic balance of the internal-wave field (e.g., Müller and Olbers, 1975; Bell, 1975). The present view of the dynamic balance is either that presented by McComas (1977) or Orlanski and Cerasoli (1980). The latter scenario is based on a plausible dissipation mechanism (using a local overturning criterion) and a numerical evaluation of the equations of motion. This yields one-dimensional spectra with liberally interpreted dependencies near those of observed spectra. It is claimed that the spectrum has reached a saturation level such that no more energy can be added to the small-scale waves without immediate loss to overturning. Our major objection to this scenario is not over the dissipation mechanism or the result of the numerical experiment, but rather the complete lack of explanation of how the dissipation mechanism acts on the spectrum and how the waves transfer energy among themselves.[3]

The McComas scenario, although identifying the transfer mechanisms, was primarily based on prejudice for a high-wavenumber sink and was inferred from the characteristics of the dominating nonlinear mechanisms. Although intuitively appealing, the proposed balance was qualitative and not rigorously supported. This paper will provide both analytic and numerical support for his scenario of generation at low wavenumbers, uniform nonlinear transfer to high wavenumbers, and dissipation there.

After discussing the basic characteristics of the observed internal-wave field in Section 2, some very minimal physical assumptions lead to a spectral model of dissipation in Section 3. From this base and the assumption of constant downscale energy flux, the wavenumber dependency of the low-frequency, near-inertial spectrum is determined in Section 4. Knowing the wavenumber dependency of inertial waves allows determination of the vertical-wavenumber and frequency dependence of the high-frequency spectrum in Section 5. Sections 4 and 5 comprise the dynamic balance of the deep-ocean internal-wave field.

In order to concentrate on the important physics and assumptions of this dynamic balance, it is presumed throughout the paper that the reader is familiar with the dominating nonlinear transfer mechanisms and their associated time scales. The validity of the weak-interaction theory will also be assumed. These topics are discussed by MB, McComas (1977) and MM.

The development of the balance is completely based on analytic approximations of the dominating mechanisms. To provide additional support, some major results are compared to a time-stepping numerical model of a weakly interacting internal-wave spectrum in Section 6. This model includes all of the possible interacting triads, not just the dominating ones. Details on the model are relegated to the Appendix. Some problems with the balance and summaries of the entire scenario are discussed in Section 7.

2. Basic characteristics of the oceanic internal wave spectrum

The dynamic balance which will be detailed in the following sections consists of a nonlinear energy transfer from a source at the energetic large scales to a dissipation range at small scales. This scenario requires certain characteristics of the internal wave spectrum which, however, fall well within the range of all observational evidence. Hence, the foundation for this balance is solid.

The general form of the one-dimensional frequency and vertical-wavenumber energy-content spectra $E(\omega)$ and $E(\beta)$ is shown in Fig. 1. Note that these spectra and all other spectra in this paper are displayed on log-log axes in the form of content spectra, such that if $\hat{E}(\beta)$ is the usual vertical-wavenumber energy-density spectrum, $E(\beta) = \beta\hat{E}(\beta)$ is the vertical-wavenumber energy-content spectrum. This content spectrum is sometimes referred to as area-preserving since $E(\beta)d(\ln\beta)$ is the energy in the logarithmic interval $d(\ln\beta)$. But, because these spectra are presented on log-log axes, the area under the curve is not representative of the energy distribution as in a linear-log representation. The representations in Fig. 1 are somewhat simplified, even from the GM models, but they encompass the salient features. The level of the spectrum is E, which for the pictured spectra is essentially the total energy in the spectrum. For the frequency spectrum, the energy is mostly at f, the inertial frequency,[4] and for the wavenumber spectrum mostly at scale β_*. The frequency spectrum falls off with slope p to the buoyancy frequency N. The wavenumber spectrum falls off with slope t. Fig. 2 shows the shear content spectrum $S(\beta) = \beta^2 E(\beta)$, which increases with slope $2\text{-}t$ to a high wavenumber cutoff β_c such that the total shear is constrained to be S. Values for the various parameters are given in Table 1 for the main thermocline at 30°N.

The spectra have been presented with these required characteristics:

1) Most of the energy is in the largest vertical scales. This, of course, is an observation. Indications are that sources generate internal wave energy at large vertical scales (e.g., Müller, 1977; Bell,

[3] Unlike surface waves, there is no observational evidence of saturation. Although the total energy is relatively constant, Orlanski and Cerasoli's "saturation" occurs at waves containing little of the energy, while the energetic waves are not saturated.

[4] For simplicity the inertial peak has been eliminated. Its presence only strengthens the assumptions of the balance.

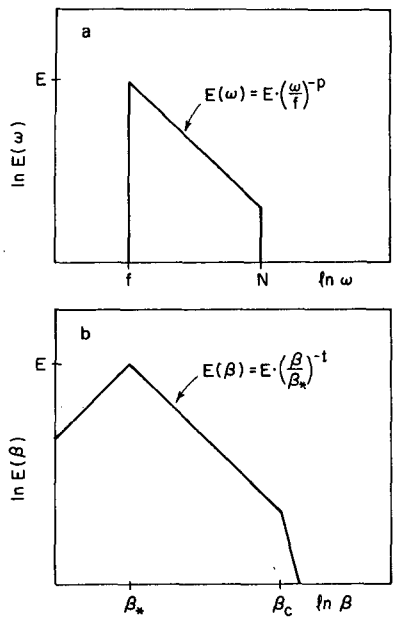

FIG. 1. Log-log representation of the one-dimensional energy-content spectra as a function of (a) frequency and (b) vertical wavenumber.

1978; Käse, 1979). Having the source at large scales, dissipation at small scales, yet most of the energy at small scales, seems unlikely. At any rate, we shall require the energy to be at large scales, i.e., $t > 0.0$.

2) Most of the shear is in the smallest vertical scales. The rate of energy-dissipation for the mechanism proposed in this paper is proportional to the shear and dissipation is assumed to be predominantly at small scales. Hence the shear must be concentrated at small scales, i.e., $t < 2.0$.

3) Most of the energy is in the lowest frequencies. For the induced-diffusion mechanism to dominate the nonlinear transfers of the higher frequency waves, the wave action E/ω must be concentrated at low frequencies. Specifically, $S(\beta, \omega)/\beta\omega$ must decrease along lines of β/ω = constant. This requires $p + t > 0$.

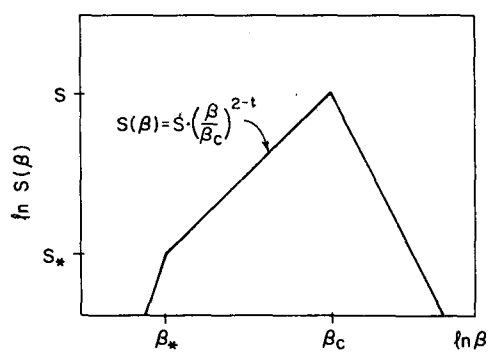

FIG. 2. Log-log representation of shear-content spectrum as a function of vertical wavenumber.

Thus, a consistent basis for the proposed balance requires $0 < t < 2$ and $p + t > 0$, or in the worst case for t, $p > 0$. Any internal-wave spectrum, oceanic, atmospheric or stellar, with these general characteristics and of sufficiently small amplitude is subject to this balance.

Oceanic observations and the GM models yield $t \in [1.0, 1.5]$ and $p \in [0.67-1.0]$, all within the required limits. Later sections will demonstrate that the vertical-wavenumber spectrum is stationary and has a uniform downscale energy flux, if $t \sim p \sim 1.0$, the GM 76 (Cairns and Williams, 1976) model values.

3. Dissipation

The observed spectrum is not in equilibrium without dissipation.[5] Unfortunately, little is known about how internal waves dissipate their energy. Shear instability (Garrett and Munk, 1972b) and gravitational instability (Orlanski and Bryan, 1969) are possible mechanisms, among others. However, there is no spectral model that specifies the scales at which dissipation occurs.

Since the information about spectral dissipation is minimal, prejudices and assumptions also should be kept at a minimum. Here we make only two basic assumptions:

- The dissipation event is localized in space and time (dimensions much smaller than the scales of the waves themselves).
- The actively mixing turbulence within each breaking event is described by a vertical eddy diffusion coefficient.

Which particular mechanism causes the dissipation events is irrelevant as long as these two conditions are met.

These assumptions mean that the mixing terms in the equation of motion for the wave field are of the form

$$\frac{d}{dt}\psi + \cdots = \partial_3 B \partial_3 \psi, \qquad (3.1)$$

[5] The statistical equilibrium solutions to the Boltzmann integral governing weak interactions without dissipation are of the form $A(\mathbf{k}) = (a\omega + \mathbf{b}\cdot\mathbf{k})^{-1}$, which is far from the observed spectrum.

TABLE 1. Basic environmental and internal wave parameters in the thermocline at 30°N.

$f = 7 \times 10^{-5}$ s^{-1}	Coriolis frequency
$N = 5 \times 10^{-3}$ s^{-1}	buoyancy frequency
$E = 3 \times 10^{-3}$ m^2 s^{-2}	total energy
$S = 2.5 \times 10^{-5}$ s^{-2}	total shear
$\beta_* = 10^{-2}$ m^{-1}	vertical wavenumber bandwidth
$S_* = 3 \times 10^{-7}$ s^{-2}	shear of energy-containing waves
$\beta_v = (S/E)^{1/2} = 10^{-1}$ m^{-1}	inverse microscale
Ri $= N^2/S = 1.0$	rms Richardson number

where

$$B = \sum_{n=1}^{N} b\delta(t - t_n)\delta(\mathbf{x} - \mathbf{x}_n) \tag{3.2}$$

and $\psi = (\mathbf{u}, \rho)$. Here $\mathbf{x}_n$ and t_n denote the locations and times of the breaking events. The coefficients for momentum and mass diffusion are the same. The coefficient b determines the strength of the turbulent diffusion within each breaking event.

Fourier transformation of (3.1) in space leads to

$$\frac{d}{dt}\psi_{\mathbf{k}} + \cdots = \frac{1}{L^3}\int_{-L/2}^{+L/2} d^3x \partial_3 B \partial_3 \psi e^{-i\mathbf{k}\cdot\mathbf{x}}$$

$$= \frac{1}{TL^3} b \sum_{\mathbf{k}'} \beta\beta' \psi_{\mathbf{k}'} \sum_{n=1}^{N} \exp[i(\mathbf{k}' - \mathbf{k})\cdot\mathbf{x}_n], \tag{3.3}$$

where the quasi-stationarity of the wave field has been invoked to introduce a time-average over a time-interval T large compared to the duration of the breaking event but small compared to the wave period. For breaking events which are not correlated with one another we can approximate (stationary-phase approximation)

$$\sum_{n=1}^{N} \exp[i(\mathbf{k}' - \mathbf{k})\cdot\mathbf{x}_n] \to N\delta_{\mathbf{k}\mathbf{k}'} \tag{3.4}$$

and find

$$\frac{d}{dt}\psi_{\mathbf{k}} = -nb\beta^2\psi_{\mathbf{k}}, \tag{3.5}$$

where $n = N/L^3T$ is the number of breaking events per unit time and volume. In the stationary-phase approximation the wave field does not distinguish between diffusion in a large number of small uncorrelated events and uniform diffusion. Corrections to the stationary-phase approximation involve intricate mathematics and reasoning (Hasselmann, 1974).

From (3.5) we find the spectral dissipation function

$$\frac{d}{dt}E(\mathbf{k}) = -\nu\beta^2 E(\mathbf{k}) = -\nu S(\mathbf{k}), \tag{3.6}$$

where

$$\nu = nb \tag{3.7}$$

is an equivalent viscosity. The spectral dissipation function is proportional to the shear spectrum. Dissipation hence occurs at the scales of the shear.

The coefficient b, in principle, can be estimated from laboratory experiments. The number n of breaking events per unit time and volume can be estimated from the statistics of the wave field. However, estimates of n (Garrett and Munk, 1972b) are extremely sensitive to the rms shear of the wave field. Hence the equivalent viscosity coefficient ν cannot reliably be estimated from definition (3.7).

Integration of (3.6) yields the overall time scale of dissipation

$$\tau_{\text{Diss}} = \frac{E}{\nu S}. \tag{3.8}$$

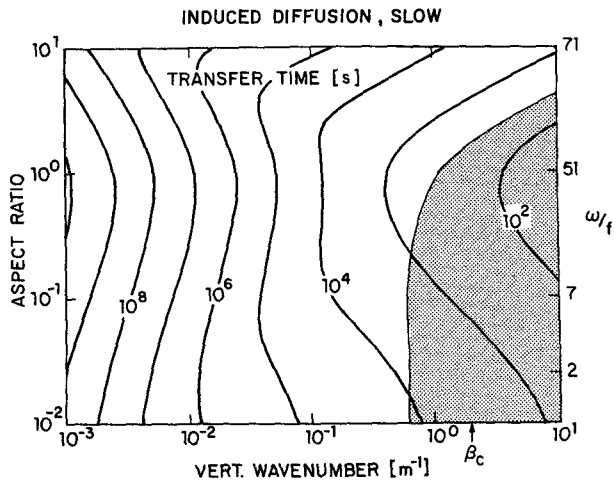

FIG. 3. Contour plot of the slow induced-diffusion time scale for the GM 76 spectral model as a function of vertical wavenumber β and normalized frequency ω/f (or aspect ratio α/β) (from MM). In the shaded area the diffusion time is smaller than the wave time scale ($\omega\tau < 1$).

An independent estimate of this time scale can be inferred from the frequency and intensity of microstructure, assuming it is caused by wavebreaking. The observations suggest the value (Garrett, 1979)

$$\tau_{\text{Diss}} \sim 100 \text{ days}$$

and hence $\nu \approx 0.14\,\text{cm}^2\,\text{s}^{-1}$ for the values in Table 1.

Using this value of the overall time scale (or viscosity coefficient) we can determine the scales at which dissipation may be considered weak in the mean. From (3.6), we find the dissipation time scale at wavenumber $\mathbf{k}$, i.e.,

$$\frac{1}{\tau(\mathbf{k})} = \nu\beta^2 = \frac{1}{\tau_{\text{Diss}}}\frac{\beta^2}{S/E}. \tag{3.9}$$

The ratio S/E defines a scale $\beta_D \sim 0.1\ \text{m}^{-1}$ such that

$$\frac{1}{\tau(\mathbf{k})} = \frac{1}{\tau_{\text{Diss}}}\left(\frac{\beta}{\beta_D}\right)^2. \tag{3.10}$$

Thus, $\tau(\mathbf{k})$ is larger than one day, the longest wave period, for wavenumbers $\beta < 10\beta_D \sim 1\ \text{m}^{-1}$. For scales larger than 1 m the dissipation is weak for inertial waves, and even weaker for higher frequency waves.

With dissipation weak at nearly all scales of interest and proportional to the spectrum (hence as smooth as the spectrum itself), the two conditions required for the validity of the slow induced-diffusion time scale (MM) are met, so the induced-diffusion mechanism is weak for wavenumbers smaller than $1\ \text{m}^{-1}$ (see Fig. 3). The parametric subharmonic

instability mechanism is also weak if $\mathrm{Ri} \gg 1$ or $\beta < \beta_c$ if $\mathrm{Ri} = 1$ (see Fig. 8 of MM).

We have constructed the simplest dissipation model we could. Assuming localized events whose mixing is described by vertical eddy diffusion coefficients, we have derived a simple model of smooth, weak energy dissipation. The effective viscosity is proportional to the total energy and inversely proportional to the total shear times the overall dissipation time scale. Microstructure observations suggest 100 days as a reasonable overall dissipation time. Such dissipation is consistent with weak nonlinear transfers for wavenumbers $< 1\ \mathrm{m}^{-1}$.

Since we insist that the shear is concentrated at small scales, dissipation is concentrated at small scales, requiring a transfer from the energetic large scales. This transfer is the subject of the next sections. However, the balances we will present do not depend on our particular dissipation model. The only requirements are that dissipation is weak and at small scales, which our model supports as reasonable assumptions.

4. The PSI balance

This section presents the balance for the low-frequency (f–$4f$) portion of the spectrum under the parametric subharmonic instability (PSI) mechanism. The assumptions are: (i) validity of weak-interaction theory; (ii) dissipation confined to small scales, and (iii) generation confined to large scales. We seek a constant-flux steady-state solution for the vertical-wavenumber dependence of the low-frequency spectrum.

The PSI mechanism is an instability wherein a low-wavenumber wave decays into two high-wavenumber waves of half the frequency. Because the dispersion relation has a different character near f, this mechanism is most effective at the lowest frequencies. The frequency resonance condition requires that the triad frequencies sum to zero, i.e., $\omega_1 + \omega_2 = \omega_3$, and since $\omega_1, \omega_2 \geq f$ the unstable wave, ω_3, must have a frequency $> 2f$. The PSI mechanism results in a downscale transfer out of the $2f$–$4f$ range into the f–$2f$ range. This section seeks to determine the scale dependence of the f–$4f$ range.

The time scale for the PSI mechanism was derived by MM and is

$$\tau^{-1}(\mathbf{k}) = \frac{27}{16}\pi f\,\mathrm{Ri}^{-1}\,\frac{S(\beta/x,\,2\omega)}{S}, \qquad (4.1)$$

where $x = [1.5f/(\omega - f)]^{1/2}$. The time scale for the growth of near inertial waves depends on the shear content of the double-frequency wave with a wavenumber x-times smaller. The factor x arises because near-inertial waves ($\mathbf{k}_1, \omega_1$) can only be generated by double-frequency waves ($\mathbf{k}_3, \omega_3$) with vertical wavenumbers $\beta_3 \leq \beta_1/x$, because of the resonance constraints. In the following we will use $x = \sqrt{10}$ (the average value of x for the GM spectral models), since the precise value of x is not crucial for our arguments.

We now assume that there is a single wavenumber dependency of the low frequency spectrum, i.e., a separable solution

$$E(\beta,\,\omega) = \frac{E(\omega)}{E}\,E(\beta) \qquad (4.2)$$

and similarly

$$S(\beta,\,2\omega) = \frac{E(2\omega)}{E}\,\beta^2 E(\beta). \qquad (4.3)$$

This assumption vastly simplifies the following derivations. Numerical calculations, presented later, show that while a separable solution is not completely valid the characteristics and results of the vertical-wavenumber balance are properly represented. With this assumption the energy gain at inertial waves is

$$\dot{E}(\beta, f) = E(\beta, f)\tau^{-1}(\beta, f) = \gamma E(f)E(\beta)E(2f)\left(\frac{\beta}{x}\right)^2 E\left(\frac{\beta}{x}\right), \qquad (4.4)$$

where

$$\gamma = \frac{27}{16}\frac{\pi f}{N^2 E^2}.$$

The energy loss at $2f$, but at the same scale β, is

$$-\dot{E}(\beta,\,2f) = \dot{E}(x\beta, f) = E(x\beta, f)\tau^{-1}(x\beta, f) = \gamma E(f)E(x\beta)E(2f)\beta^2 E(\beta). \qquad (4.5)$$

This is the loss of energy to inertial waves with wavenumbers x times larger (see Fig. 4).

If we require a steady state solution at any β, then the loss from the double-frequency wave at β must balance the gain of the half-frequency wave, also at β, i.e.,

$$\dot{E}(\beta, f) + \dot{E}(\beta,\,2f) = 0. \qquad (4.6)$$

Substituting (4.4) and (4.5) into (4.6) we then find

$$x^{-2}E\left(\frac{\beta}{x}\right) = E(x\beta). \qquad (4.7)$$

For any value of x this functional relationship has as the only nontrivial solution a power law with slope $t = 1.0$, i.e.,

$$E(\beta) \propto \beta^{-1}. \qquad (4.8)$$

This demonstration used the PSI mechanism for f and $2f$ waves, but it is obviously extendible to waves of any frequencies ω and 2ω where the PSI mechanism dominates. We therefore have shown that the low-frequency (f–$4f$) wavenumber *content* spectrum is in equilibrium under the PSI mechanism if $E(\beta) \propto \beta^{-1}$ as in GM 76.

Because the transfers under the PSI mechanism are contained exclusively in the f–$4f$ region, a one-dimensional wavenumber energy flux may be defined by

$$\frac{\partial}{\partial t}\hat{E}(\beta) + \frac{\partial}{\partial \beta}\hat{Q}(\beta) = 0, \tag{4.9}$$

where $\hat{E}(\beta) = \beta^{-1}E(\beta)$ is the vertical-wavenumber energy *density* spectrum. Since $\partial/\partial t E(\beta) = 0$, $\partial/\partial t \hat{E}(\beta) = 0$, and the energy flux $\hat{Q}(\beta)$ is constant.

The flux $\hat{Q}(\beta)$ is determined at either the low-wavenumber end, near β_*, or at the high-wavenumber end, near β_c. For wavenumbers $\beta < \beta_*$ the shear drops off quickly, so that for near-inertial waves with $\beta < \beta_*$ the PSI mechanism is ineffective. Hence a good estimate of the flux across $\beta = \beta_*$ is

$$\hat{Q}(\beta_*) = -\int_0^{\beta_*} d\beta \frac{\partial}{\partial t}\hat{E}(\beta, 2f) \approx -\dot{E}(\beta_*, 2f)$$
$$= \gamma E(f)E(2f)E(x\beta_*)S(\beta_*). \tag{4.10}$$

For $\beta > \beta_c$, again the shear drops off rapidly, so that the loss from the region $2f$–$4f$ for waves with $\beta > \beta_c$ is ineffective. A good estimate of the flux across $\beta = \beta_c$ is then

$$\hat{Q}(\beta_c) = \int_{x\beta_c}^{\infty} d\beta \frac{\partial}{\partial t}\hat{E}(\beta, f) = \dot{E}(x\beta_c, f)$$
$$= \gamma E(f)E(x\beta_c)E(2f)S(\beta_c). \tag{4.11}$$

If the flux is constant between β_* and β_c, as (4.9) indicates, then

$$\hat{Q}(\beta_*) = \hat{Q}(\beta_c) \tag{4.12}$$

or

$$\frac{E(x\beta_c)}{E(x\beta_*)} = \frac{S(\beta_*)}{S(\beta_c)} \tag{4.13}$$

or, liberally,

$$\frac{E(\beta_c)}{E} \approx \frac{S_*}{S}, \tag{4.14}$$

where $S_* = S(\beta_*) = \beta_*{}^2E$ is the shear of the energy-containing waves, $E = E(\beta_*)$ the total energy, and $S = S(\beta_c)$ the total shear. Eq. (4.14) is a condition on the energy level at β_c,[6] given E, S and S_* or equivalently, a determination of the width of the constant-energy-flux range, if the spectral slope t and $\beta_D{}^2 \equiv S/E$ are known, i.e.,

$$\frac{\beta_c}{\beta_*} = \left(\frac{\beta_D}{\beta_*}\right)^{2/t}. \tag{4.15}$$

This is a kinematic constraint determining the scale

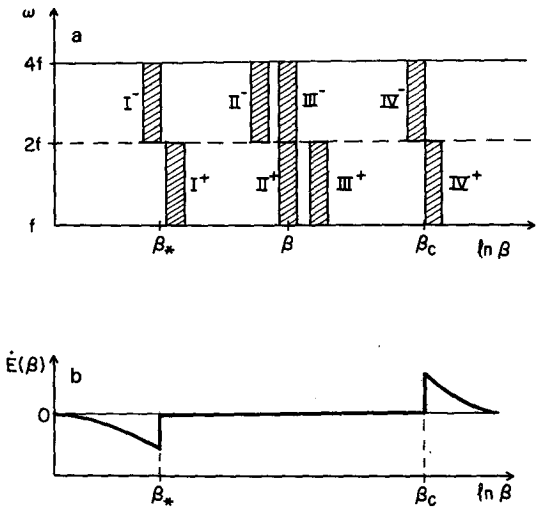

FIG. 4. The PSI mechanism. (a) At the energy scale β_*, energy is transferred from region I^- into I^+ creating a flux across β_*. There is no compensating gain beneath I^- because the shear spectrum falls off rapidly for $\beta < \beta_*$. At arbitrary β where $\beta_* < \beta < \beta_c$, II^- transfers energy to II^+, III^- to III^+, and so on. Since $III^- + II^+ = 0$ the spectrum is in equilibrium. For $\beta > \beta_c$ the shear and energy spectrum falls off so that IV^+ is not balanced, resulting in a flux across β_c. (b) Schematic representation of the rate of change of energy as a function of vertical wavenumber under the PSI mechanism.

β_c at which the constant-flux solution reaches total shear S. For $t = 1.0$, β_D and β_* as in Table 1, we find $\beta_c/\beta_* \sim 100$.

A simplification of (4.1) for $E(\omega) = E\cdot(\omega/f)^{-1}$ shows that the constant flux is

$$\hat{Q} \approx \frac{E}{\tau_*} \approx \frac{27}{32x}\frac{\pi f}{N^2}ES_*, \tag{4.16}$$

proportional to the energy times the shear content of the source region. The bandwidth of the source region is just as important as the level in determining the energy flux. Both dependencies are quadratic, so that a factor-10 change in either results in a 100-fold change in the energy flux.

This flux should be of the proper magnitude to balance dissipation at scales smaller than $\beta_c{}^{-1}$, i.e.,

$$\hat{Q}(\beta_*) = \int_{\beta_c}^{\infty} d\beta \dot{E}_{\text{Diss}}(\beta). \tag{4.17}$$

If dissipation is confined to scales smaller than $\beta_c{}^{-1}$, then the integral is equal to E/τ_{Diss}. Since $\hat{Q}(\beta_*) = E/\tau_*$, the flux always matches the dissipation if

$$\tau_{\text{Diss}} = \tau_*, \tag{4.18}$$

i.e., if the overall dissipation time scale equals the time scale for the PSI mechanism to move energy out of the energetic scales. This result is independent of the dissipation distribution.

From (4.1) we find

[6] If $E(\beta) = E\cdot(\beta/\beta_*)^{-t}$ and hence $S(\beta) = S_*\cdot(\beta/\beta_*)^{2-t}$ then (4.14) requires $t = 1.0$. This is an equivalent proof of $t = 1.0$ as the constant-flux solution under the PSI mechanism.

$$\tau_*^{-1} = \frac{27}{16}\pi\frac{f}{N^2}S\left(\frac{\beta_*}{x}, 2f\right) \approx \frac{27}{32}\pi\frac{f}{N^2}\frac{\beta_*^2}{x}E \quad (4.19)$$

if $E(\omega) = E\cdot(\omega/f)^{-1}$ which for values in Table 1 gives $\tau_* \sim 50$ days. This is comparable to the estimate $\tau_{\text{Diss}} \approx 100$ days of Garrett (1979).

Conversely, if τ_{Diss} and E are regarded as known, condition (4.17) specifies the absolute location of the constant-flux region, i.e.,

$$\beta_* = \left[\frac{27}{32}\frac{\pi f}{xN^2}E\tau_{\text{Diss}}\right]^{-1/2}. \quad (4.20)$$

For values in Table 1 and $\tau_{\text{Diss}} = 100$ days we find $\beta_* = 4 \times 10^{-3}$ m^{-1}, also satisfying within our overall accuracy.

At some scale $\tilde{\beta}_c$ the transfer by the PSI mechanism just balances the dissipation. For $\beta < \tilde{\beta}_c$ transfer easily exceeds dissipation; for $\beta > \tilde{\beta}_c$ the dissipation in a constant-flux spectrum exceeds the maximum transfer. Clearly, for $\beta > \tilde{\beta}_c$, the constant-flux inertial range cannot survive and the spectrum must fall off. The point at which this occurs is where $\tau_{\text{Diss}} = \tau_{\text{PSI}}$ or

$$\frac{\tilde{\beta}_c}{\beta_*} = \frac{\tau_{\text{Diss}}}{\tau_*}\frac{S}{S_*}. \quad (4.21)$$

If $\tau_{\text{Diss}} = \tau_*$ as (4.17) implies it must, then $\tilde{\beta}_c = \beta_c = \beta_* S/S_*$ and the dissipation *forces* the constant-flux spectrum to cut off at β_c with total shear S, consistent with (4.15) for $t = 1.0$. For values in Table 1 we find $\beta_c \approx 1$ m^{-1}, which is just the wavenumber around which observed temperature (e.g., Gregg, 1977) and velocity (e.g., Gargett *et al.*, 1981) spectra show an elbow or change in slope.

Clearly, β_c is determined by features of the source region, i.e., β_* and E. As the source region grows, the flux increases, the dissipation increases (the equivalent viscosity increases) and the separation between energetic and dissipative scales decreases (as long as the total shear remains constant). If we know the overall dissipation time scale, τ_{Diss} and the total energy, E, then Eqs. (4.20) and (4.21) determine the scales of the constant-flux inertial range $\beta \in [\beta_* \beta_c]$.

To recapitulate the essentials of this PSI balance: we have assumed the energy and sources to be at large scales $\beta < \beta_*$. The dissipation occurs at small scales $\beta > \beta_c$ such that the total shear is S. Between these two regions we have presumed an inertial cascade. We found the following:

1) The wavenumber spectrum has the form $E(\beta) = E\cdot(\beta/\beta_*)^{-1}$

2) The constant flux $\hat{Q}$ is a quadratic function of E and β_*.

3) The cutoff scale β_c is determined by E, β_* and S

4) The dissipation time must equal the time scale to move energy out of the energetic scales, $\tau_{\text{Diss}} = \tau_*$.

The above four points imply that if one knows E and β_*, then one also knows $E(\beta)$, $\hat{Q}(\beta)$, β_c and τ_{Diss}! Conversely, if one knows E and τ_{Diss}, then one also knows the others. The internal-wave model we present here has only three parameters, E, β_* and S. Presumably, S is constant, while E and β_* have time scales of the order of 100 days. Thus the gross features of the internal-wave field evolve slowly. Knowing two rough measures of the energetic scales, E and β_*, specifies the rest of the internal-wave spectrum. (The high-frequency dependence is determined in the next section.)

Eqs. (4.16) and (4.21) should be verifiable by experiment, at least qualitatively. The quantities E and β_* are available from vertically separated current meters and β_c from small-scale profiles. Changes in E and β_* should then correspond to changes in the occurrence and intensity of microstructure and to changes in β_c, assuming $S = \tilde{N}$. Since E and β_* evolve on time scales of the order of 100 days these correspondences should be most apparent in long records and in the geographical distribution of these quantities.

5. The ID balance

This section presents the balance for the high-frequency spectrum, $4f \leqslant \omega \ll N$, which interacts with the low-frequency inertial band under the induced diffusion (ID) mechanism. The assumptions are the same as in the previous section. The approach is also the same. We seek a steady-state solution for the vertical-wavenumber spectrum.

The ID mechanism is the scattering of a high-frequency high-wavenumber wave by a low-frequency low-wavenumber wave. It acts as a diffusion of wave action in wavenumber space, primarily in vertical wavenumber. The diffusion coefficient is proportional to the shear content of the low-frequency wave. Wave action is conserved in the high frequency region and its rate of change at any wavenumber $\mathbf{k}$ is given by (MM)

$$\frac{\partial}{\partial t}\hat{A}(\mathbf{k}) = \frac{\partial}{\partial\beta}D\frac{\partial}{\partial\beta}\hat{A}(\mathbf{k}), \quad (5.1)$$

where

$$D = \tfrac{1}{2}\pi f^{-1}\alpha^2 S\left(\frac{f}{\omega}\beta\right) \quad (5.2)$$

is the diffusion coefficient, and $\hat{A}(\mathbf{k})$ is the three-dimensional action-density spectrum. The diffusion coefficient is generally a function of β through the shear content of the low-frequency waves.

Eq. (5.1) implies an action flux in vertical wavenumber along a line of constant horizontal wave-

number α given by

$$\hat{Q}_A(\mathbf{k}) = -D \frac{\partial}{\partial \beta} \hat{A}(\mathbf{k}), \tag{5.3}$$

with a corresponding energy flux

$$\hat{Q}_E(\mathbf{k}) = \omega \hat{Q}_A(\mathbf{k}). \tag{5.4}$$

From (5.1), the rate of change of the energy density in the high-frequency spectrum can be related to the energy flux by

$$\frac{\partial}{\partial t} \hat{E}(\alpha, \beta) + \frac{\partial}{\partial \beta} \hat{Q}_E(\alpha, \beta) + \frac{1}{\beta} \hat{Q}_E(\alpha, \beta) = 0, \tag{5.5}$$

since $\partial\omega/\partial\beta \sim -\omega/\beta$ at high frequencies. Clearly, if $\hat{Q}_E$ is uniform,[7] the time rate of change of the energy in the high-frequency region is *not* zero. If $\hat{Q}_E(\alpha, \beta) \geq 0$, then $\partial/\partial t \hat{E}(\alpha, \beta) \geq 0$ and energy is lost from the high-frequency region. For a similar discussion of a uniform action flux see Fig. 5. The energy in the high-frequency region alone is not conserved or, in general, constant (if $\hat{Q}_A \neq$ uniform).

The "lost" energy, of course, is gained by the low-frequency waves (see Fig. 6). Previous attempts to find equilibrium solutions under the ID mechanisms (MM; McComas, 1978; McComas and Bretherton, 1977) ignored this energy transfer and sought solutions only for the high-frequency region. Here, we include both regions and look for equilibrium solutions for the combination of these two regions.

The time rate of change of the low-frequency energy-density spectrum is given by

$$\frac{\partial}{\partial t} \hat{E}_L(\beta) = \beta^{-1} \int \hat{Q}_E(\alpha, \beta') d\alpha, \tag{5.6}$$

where $\beta' = \beta\omega/f = \beta N\alpha/f\beta'$. This equation is derived from the full Boltzmann equation using the characteristics of the ID triad as done by MM.

Addition of (5.6) to an integration of (5.5) over α yields the equation for the time rate of change of the vertical-wavenumber spectrum

$$\frac{\partial}{\partial t} \hat{E}(\beta) + \frac{\partial}{\partial \beta} \hat{Q}_E(\beta) = \int d\alpha \beta^{-1} [\hat{Q}_E(\alpha, \beta') - \hat{Q}_E(\alpha, \beta)], \tag{5.7}$$

where

$$\hat{Q}_E(\beta) = \int d\alpha \hat{Q}_E(\alpha, \beta),$$

$$\hat{E}(\beta) = \hat{E}_L(\beta) \int \hat{E}(\alpha, \beta) d\alpha.$$

If the energy flux is uniform, i.e., $\hat{Q}_E(\alpha, \beta) = F(\alpha)$,

[7] The word uniform means here and in the following: independent of the vertical wavenumber β.

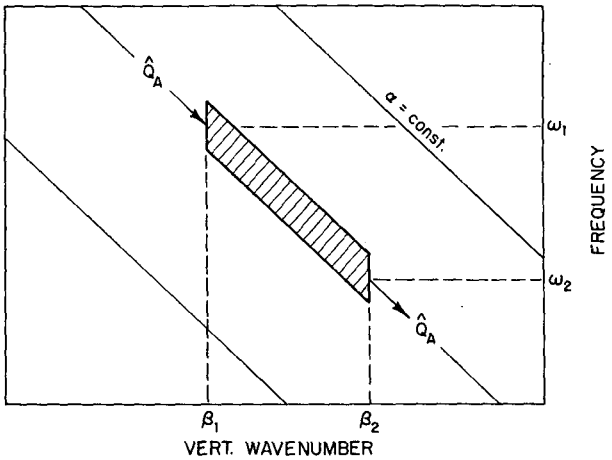

FIG. 5. The uniform-action-flux solution. At $\beta_1 < \beta_2$, a uniform-action flux $\hat{Q}_A$ enters the region. The energy flux is $\omega_1\hat{Q}_A$. The same action flux leaves the region at β_2, and action is conserved, i.e., $\partial\hat{A}/\partial t = 0$. The energy flux out of the region is $\omega_2\hat{Q}_A$, but since $\omega_2 < \omega_1$ (because $\beta_2 > \beta_1$ and α is constant), the energy flux out of the region is smaller than that entering. But since $\partial\hat{A}/\partial t = 0$ the energy content in the region also must be constant, i.e., $\partial\hat{E}/\partial t = 0$. Thus energy must be transferred out of the region to balance the non-constant energy flux [the third term in (5.5)].

both the right-hand side of (5.7) and the divergence of $\hat{Q}_E(\beta)$ vanish; hence $\hat{E}(\beta)$ is stationary, i.e.,

$$\frac{\partial}{\partial t} \hat{E}(\beta) = 0. \tag{5.8}$$

Thus, the vertical-wavenumber energy-density spectrum is in equilibrium under the ID mechanism if the energy flux through the high-frequency region is uniform. This is the principal result of this section.

We now determine the high-frequency spectrum which has the uniform flux $\hat{Q}_E(\alpha, \beta) = F(\alpha)$. A complete solution of the diffusion equation (5.1) requires two boundary conditions. The obvious boundary conditions are that the energy spectrum and the time rate of change of the energy spectrum are continuous at the boundary between the PSI and ID regions.

The action-density spectrum can be determined from an integration of (5.3), i.e.,

$$\hat{A}(\alpha, \beta) = -\frac{F(\alpha)}{\frac{1}{2}\pi\alpha^2} \cdot \times \left[\int_{\beta_z}^{\beta} d\beta' \frac{1}{(\omega/f) S(\beta' f/\omega)} - \frac{\beta_*}{S_*} C(\alpha) \right]. \tag{5.9}$$

If we insist that the wavenumber dependence of the low-frequency shear is determined by the PSI mechanism, then

$$S(\beta) = S_* \frac{\beta}{\beta_*}, \tag{5.10}$$

so that

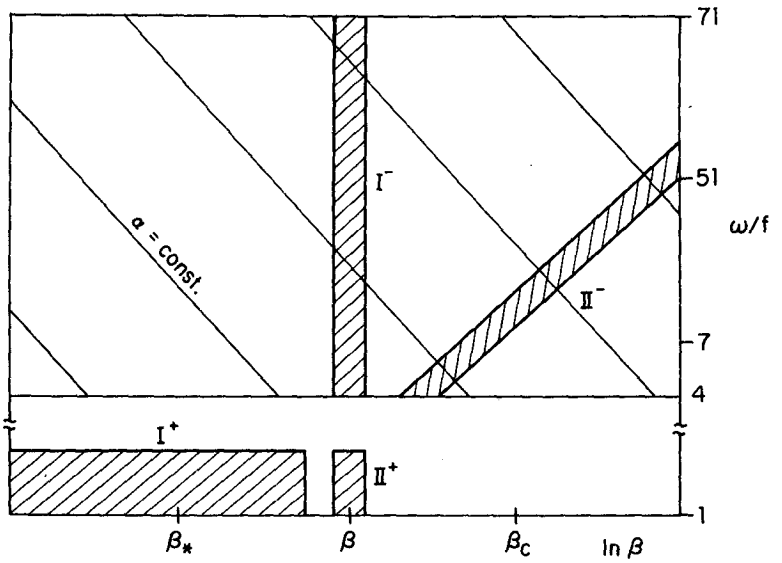

FIG. 6. The ID mechanism. At wavenumber β energy is lost out of the high-frequency region I^-. This energy is gained by the low-frequency region I^+, consisting of near inertial waves with vertical wavenumbers $\beta' = (f/\omega)\beta$. The energy gain in the region II^+ comes from the region II^- consisting of high-frequency waves with vertical wavenumbers $\beta' = (\omega/f)\beta$. Stationarity of the vertical-wavenumber spectrum at β requires $II^+ + I^- = 0$ which implies a uniform energy flux through the high-frequency region.

$$\hat{A}(\alpha, \beta) = -\frac{F(\alpha)\beta_*}{\tfrac{1}{2}\pi S_* \alpha^2}\left[\ln\frac{\beta}{\beta_*} - C(\alpha)\right]. \quad (5.11)$$

The functions $F(\alpha)$ and $C(\alpha)$ are integration constants of the vertical-wavenumber diffusion problem that are evaluated by the boundary conditions.

The first condition matches the rates of change of the spectrum. From (5.5) the ID rate is

$$\frac{\partial}{\partial t}\hat{E}_{ID}(\alpha, \beta) = -\frac{F(\alpha)}{\beta} \quad (5.12)$$

or

$$\frac{\partial}{\partial t}E_{ID}(\omega, \beta) = \frac{\omega\beta}{|\partial\omega/\partial\alpha|}\frac{\partial}{\partial t}\hat{E}_{ID}(\alpha, \beta) = -\alpha F(\alpha). \quad (5.13)$$

This rate is set equal to the time rate of change under the PSI mechanism at the common boundary, which is chosen at $\omega \sim 4f$. Similar to (4.5), the PSI rate is given by (MM)

$$\frac{\partial}{\partial t}E_{PSI}(4f, \beta) \sim -\gamma E(2f)E(x\beta)E(4f)\beta^2 E(\beta) \approx -\gamma\frac{E^4\beta_*^2}{8x} \equiv -\gamma', \quad (5.14)$$

if we take $E(\omega) = E\cdot(\omega/f)^{-1}$ for definiteness, and $E(\beta) = E\cdot(\beta/\beta_*)^{-1}$, the constant-flux solution for the PSI region. Thus the energy change along a line of constant frequency is uniform.

Setting (5.13) and (5.14) equal determines $F(\alpha)$

$$F(\alpha) = \frac{\gamma'}{\alpha}. \quad (5.15)$$

Note that $F(\alpha)$, the vertical-wavenumber energy flux, is positive, implying a downscale flux. Further, since γ' can be rewritten as $\gamma' = (27/128x)(\pi f/N^2)ES_*$, this downscale energy flux is proportional to the energy level times the shear level of the energy-containing region, just as was the PSI flux (4.16).

To determine $C(\alpha)$ the energy spectra are matched. If we take the low-frequency spectrum to be

$$E_L(\omega, \beta) = \frac{E}{\omega/f}\frac{1}{\beta/\beta_*} \quad (5.16)$$

and match it to the solution

$$E_{ID}(\omega, \beta) = \frac{\omega^2\beta}{|\partial\omega/\partial\alpha|}\hat{A}(\alpha, \beta) \quad (5.17)$$

along the line $\omega = 4f$, we find

$$C(\alpha) = \frac{64x}{27} + \ln\frac{N}{4f}\frac{\alpha}{\beta_*}. \quad (5.18)$$

Combining (5.11) with (5.15) and (5.18) gives the complete description of the high-frequency spectrum in terms of the energy level and bandwidth of the large-scale waves:

$$E_{ID}(\omega, \beta) = E \cdot \left(\frac{\beta}{\beta_*}\right)^{-1} \left(\frac{\omega}{f}\right)^{-1} \left[1 + \frac{27}{64x} \ln \frac{\omega}{4f}\right]. \quad (5.19)$$

If one matches the energy spectra along $\beta = \beta_*$, one finds

$$E_{ID}(\omega, \beta) = E \cdot \left(\frac{\beta}{\beta_*}\right)^{-1} \left(\frac{\omega}{f}\right)^{-1} \left[1 - \frac{27}{64x} \ln \frac{\beta}{\beta_*}\right].$$

Except for the logarithmic correction, the solution describes a power-law dependence with respect to frequency and vertical wavenumber, both with slope -1. We hence see that the assumed frequency dependence of the PSI mechanism, $E(\omega) = E \cdot (\omega/f)^{-1}$ is merely an extension of the frequency dependence of the ID solution. The first term in (5.19) is the no-flux term, the second the uniform-energy-flux term.

In deriving the high-frequency solution we did not mention dissipation explicitly, since dissipation is very weak at all scales of interest. The time rate of change of energy under the ID mechanism

$$\frac{\partial}{\partial t} \hat{E}_{ID}(\alpha, \beta) = -\frac{F(\alpha)}{\beta} \quad (5.20)$$

is proportional to $1/\beta$ while the dissipation rate

$$\frac{\partial}{\partial t} \hat{E}_{Diss}(\alpha, \beta) = -\nu \hat{S}(\alpha, \beta) = -\nu \beta^2 \hat{E}(\alpha, \beta) \quad (5.21)$$

is proportional to β. We may define a β_c' such that for $\beta < \beta_c'$, $|\dot{E}_{ID}| > |\dot{E}_{Diss}|$, and for $\beta > \beta_c'$, $|\dot{E}_{Diss}| > |\dot{E}_{ID}|$. That β_c' is where $|\dot{E}_{Diss}| = |\dot{E}_{ID}|$ or

$$\frac{\beta_c'}{\beta_*} = \frac{27\pi}{128x} \mathrm{Ri}^{-1} \tau_{Diss} \omega. \quad (5.22)$$

For $\mathrm{Ri} = 1$ and $\omega = 4f$

$$\frac{\beta_c'}{\beta_*} = 500 \quad (5.23)$$

which makes β_c' considerably larger than the maximum wavenumbers we considered and at which our weak-interaction theory applies.

Although one might argue about some of the numerical constants, or whether the boundary between the PSI and ID regions should be at $\omega = 4f$ or $5f$, the following points made in this section are well founded:

1) The vertical wavenumber spectrum has stationary solutions under the ID mechanism with a uniform downscale energy flux.

2) By matching the ID solution to the low-frequency spectrum one of the stationary solutions is selected. This particular solution has a flux proportional to the energy level times the shear of the large-scale waves, as does the PSI flux.

3) The spectral solution, except for the small magnitude, weak logarithmic dependence on ω, has the same ω, β dependence as the observationally based GM 76 model.

4) The difference between the flux and no flux diffusion solution is small (<30% at $\omega = N/2$) and presumably unobservable.

6. A numerical model

The most important result of the previous sections was the demonstration of a stationary vertical-wavenumber spectrum with a constant downscale energy flux. To obtain this result, we had to assume that the low-frequency (f–$4f$) range could be described by a single vertical-wavenumber dependence and an unspecified frequency dependence, i.e.,

$$E(\omega, \beta) = \frac{E(\omega)}{E} E(\beta). \quad (6.1)$$

Clearly, such a spectral description is not possible under the PSI mechanism alone, as the f–$2f$ region gains energy, and the $2f$–$4f$ region loses that energy such that $E(\omega)$ could not be stationary. Further, the PSI time scale is not independent of vertical wavenumber if $E(\beta) \propto \beta^{-1}$, so that $E(\omega, \beta)$ would not long remain proportional to β^{-1} at every frequency.

For the ID mechanism, the constant downscale flux idea is well founded. However, to solve for a specific functional form in α, we had to match to the PSI region. The specific solution we obtained depends in its particulars on the presumed form of the low-frequency spectrum.

In order to confirm our scenario and support our assumptions about the low-frequency range we have developed a time-stepping numerical model which computes the evolution of the internal-wave spectrum from an accurate determination of all the interacting triads. We have used the dissipation model developed in Section 3 and initial spectra from the GM 76 model. Model runs were performed on the Cray computer at the National Center for Atmospheric Research. Because of the extremely wide separation between the characteristic time scale of the energy-containing waves and the stability time scale of the diffusing high-shear waves (a factor of almost 10^5), only a few, unsatisfyingly short computations were performed on account of the expense. However, these calculations do demonstrate all of the characteristics of our constant-flux scenario, and should ease any concerns regarding some of our assumptions about the low-frequency range. In our view, the analytic model without the numerical result is less convincing; the numerical result without the simple framework for understanding provided by the analytic model is nearly useless.

We relegate some details of the numerical model to the Appendix, and mention here only those points

TABLE 2. Basic environmental and internal-wave parameters of numerical model.

Constant values		
N	4.5×10^{-3}	s^{-1}
f	7.0×10^{-5}	s^{-1}
ρ_*	7.0×10^{-3}	m^{-1}
ν	4.0×10^{-2}	$cm^2\ s^{-1}$

Nearly constant values	0 days	14 days	28 days
E_{TOT} ($cm^2\ s^{-2}$)	1.43×10^{1}	1.41×10^{1}	1.40×10^{1}
E_* ($cm^2\ s^{-2}$)	6.2×10^{0}	6.1×10^{0}	6.1×10^{0}
S_* (s^{-2})	3.1×10^{-8}	3.1×10^{-8}	3.1×10^{-8}
S_{TOT} (s^{-2})	3.1×10^{-6}	2.8×10^{-6}	2.4×10^{-6}
$\beta_D^2 = \frac{S_{TOT}}{E_*}$ (m^{-2})	5.0×10^{-3}	4.6×10^{-3}	4.0×10^{-3}

needed to understand and apply the results to the scenario of the previous sections.

The initial spectrum is a slightly modified GM 76 spectrum of the form

$$E_0(\omega, \rho) = E_* A(\omega) B(\rho), \tag{6.2}$$

where $\rho \equiv |\mathbf{k}|$ (the wavenumber magnitude), $A(\omega) = (\omega/f)^{-1}$, and $B(\rho) = (1 + \rho/\rho_*)^{-1}$. The one-dimensional spectra are then

$$E_0(\omega) = E_{TOT} A(\omega), \tag{6.3}$$

where $E_{TOT} = 2.3 \cdot E_*$ is the total energy and

$$E_0(\rho) = E_* B(\rho). \tag{6.4}$$

The principal modification to the GM 76 model is in $B(\rho)$. We used ρ instead of β, and modified the energy-containing scales such that the energy content, instead of increasing towards ρ_*, is relatively flat. This change allows a greater E_{TOT} for the same E_*, but alters little else.

Table 2 presents the constant and nearly constant values in the model. We have chosen ν such that

$$\tau_{Diss} = \frac{E_*}{S_{TOT}\nu} = 5 \times 10^7\ s \approx 500\ days \tag{6.5}$$

to match the PSI time scale out of the energy containing scales [see Eq. (4.18)]

$$\tau_* = \frac{16}{27}\frac{N^2}{\pi f}\frac{1}{S(\beta_*/x, 2f)} \approx 500\ days. \tag{6.6}$$

We expect the spectral break point β_c at

$$\frac{\beta_c}{\beta_*} = \left(\frac{\beta_D}{\beta_*}\right)^2 = 10^{2.0} \tag{6.7}$$

by Eq. (4.15).

The dissipation is given by

$$\dot{E}_{Diss}(\rho, \omega) = -\nu S(\rho, \omega) = -\nu\rho^2 E(\beta, \omega), \tag{6.8}$$

while the transfer into the inertial band under the PSI mechanism is given by

$$\dot{E}_{PSI}(\rho, f) = \frac{27}{16}\frac{\pi f}{N^2} S(\beta/x, 2f) E(\rho, f)$$

$$= \frac{1}{\tau_*} E(\rho, f) S(\beta/x, 2f)/S(\beta_*/x, 2f). \tag{6.9}$$

For the constant flux solution $\tau_{PSI}^{-1}(\beta, f) \propto \beta$, while $\tau_{Diss}^{-1}(\beta, f) \propto \beta^2$. At some scale β_c the dissipation time scale equals the PSI transfer time. For $\beta > \tilde{\beta}_c$ dissipation dominates transfer and vice versa. That $\tilde{\beta}_c$ is

$$\frac{\tilde{\beta}_c}{\beta_*} = \frac{\tau_{Diss}}{\tau_*}\frac{S_{TOT}}{S_*} \tag{6.10}$$

as we found in (4.21). The two scales β_c and $\tilde{\beta}_c$ are equal if $\tau_{Diss} = \tau_*$, which we have already assured. This match is important because it is the dissipation that assures that the spectrum cuts off at $\tilde{\beta}_c$. The scale β_c is only that scale where the constant-flux spectrum reaches the total shear value S_{TOT}. The β_c is a kinematic constraint, while $\tilde{\beta}_c$ is a dynamic one.

In the model, the spectrum is represented on a 13×13 grid in $\log_{\sqrt{2}}\omega/f$ versus $\log_{10}\rho$ space. The variables range over $1 \leq \omega/f \leq 64 = N/f$ and $10^{-3} \leq \rho \leq 1\ m^{-1}$. There are 144 "bins" in the model, each having a logarithmic interval, e.g., $bin_{3,5}$ contains $2f \leq \omega \leq 2\sqrt{2}f$ and $10^{-2.0}\ m^{-1} \leq \rho \leq 10^{-1.75}\ m^{-1}$. All interactions and dissipation occur within the variable ranges. Interactions conserve energy to machine accuracy ($\sim$1 part in 10^{10}). The model results will be presented in terms of various one-dimensional energy content spectra.

We begin by showing the time evolution over 28

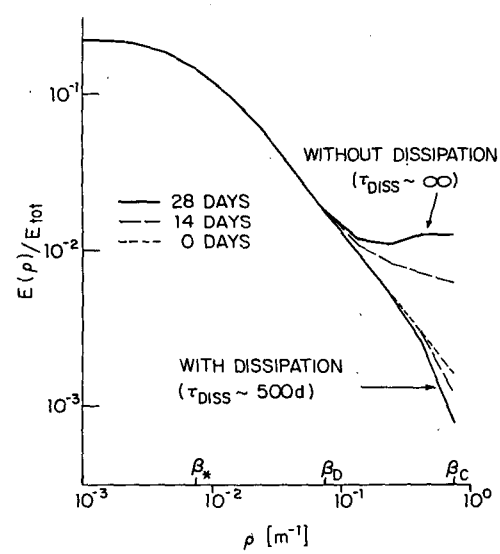

FIG. 7. The wavenumber spectrum for $\tau_{Diss} = \infty$ and for $\tau_{Diss} = 500$ days at 0, 14 and 28 days.

days of the vertical-wavenumber energy-content spectrum in Fig. 7. Here we show one run with no dissipation. Note that the higher wavenumbers have filled appreciably, increasing the shear dramatically. Clearly, the presence of small-scale dissipation is crucial to the maintenance of the oceanic spectrum.

The second set of curves describes the evolution of the spectrum with $\nu = 0.04$ cm^2 s^{-1}. The initial slope is maintained until the last bin where

$$\frac{\rho}{\rho_*} \approx \frac{\beta}{\beta_*} = 10^{2.0},$$

confirming the predictions of (6.10) and (6.7) for the cutoff wavenumber. Fig. 8 shows the time scale for the vertical-wavenumber spectrum in each "bin." Note that for small-scale waves, $\beta = O(10^{-1}\ \mathrm{m}^{-1})$, the one-dimensional spectrum has a time scale of order 10^3 days. This is much longer than the characteristic time scale for the PSI mechanism or the ID mechanism found by MM, indicating the equilibrium in the one-dimensional spectrum.

Fig. 9 shows the time rate of change of the wavenumber spectrum, $\dot{E}(\rho)$, and the time rate of change of the wavenumber spectrum of bin 1, $f \leq \omega \leq \sqrt{2}\omega$, $\dot{E}_1(\rho)$. The rate $\dot{E}_1(\rho)$ includes both the nonlinear transfer and the dissipation in that bin. At high wavenumbers the rates $\dot{E}_1(\rho)$ are greater than the rates $\dot{E}(\rho)$, which means that the increase in the inertial bin 1 is offset by higher frequency bands. Also shown is the total dissipation, which is dominated by the low-frequency bin 1. If dissipation is subtracted from the rate $\dot{E}_1(\rho)$, it can easily be seen that the transfer

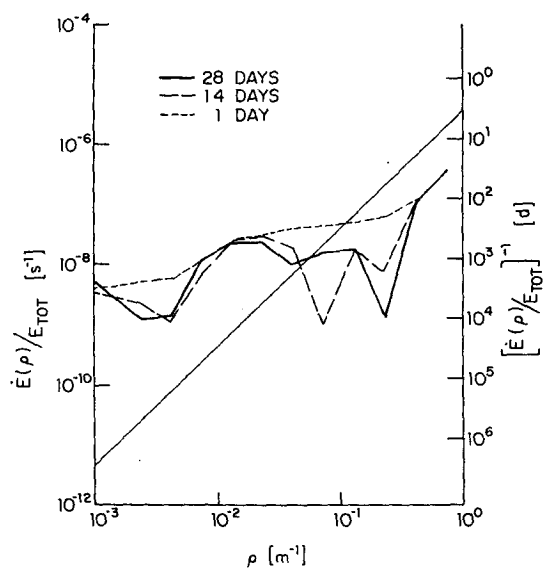

FIG. 8. Time scales of the wavenumber spectrum at 1, 14 and 28 days. The straight line represents the dissipation time scale $\tau_{Diss}^{-1}(\rho) = \nu\rho^2$.

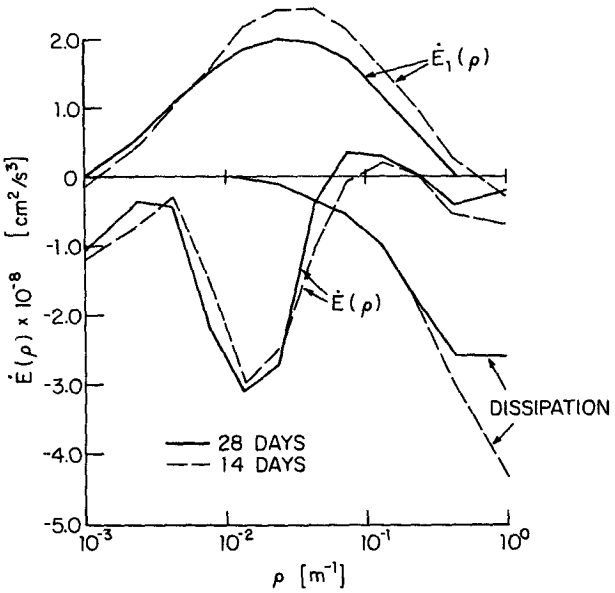

FIG. 9. The energy transfer rates for the wavenumber spectrum $\dot{E}(\rho)$, the energy transfer rates for bin 1, $f \leq \omega \leq \sqrt{2}f$, $\dot{E}_1(\rho)$, and the dissipation function $\dot{E}_{Diss}(\rho) = -\nu\rho^2 E(\rho)$ at 14 and 28 days.

into bin 1 is nearly independent of wavenumber, as predicted by (4.4) and (5.14); it only changes by about a factor of 2 over two decades of wavenumbers. This wavenumber independence is the crucial point in the determination of $F(\alpha)$ under the ID mechanism in (5.15).

We next investigate our assumed PSI form (6.1) and its attendant difficulties. Fig. 10a shows the evolution of the wavenumber spectrum of frequency bin 1. The spectrum is increasing in energy as the PSI mechanism transfers energy into the inertial band. Because the time scale is proportional to β, this causes the wavenumber spectrum of bin 1 to become less steep. But, at the end of our computer simulation, there is an indication that the rate of increase at the smallest waves is decreasing, indicating that the spectrum begins to flatten out again as the inertial peak is sufficiently built up.

Fig. 10b shows the evolution of the spectrum for bin 3, which is bin 1's PSI partner, i.e., bin 3 loses under the PSI mechanism what bin 1 gains. We see that the loss from bin 3 follows the same pattern as the gain of bin 1.

Fig. 10c shows the evolution of the sum of bins 1 to 4, i.e., $f \leq \omega \leq 4f$. The spectrum remains quite close to the initial spectrum. The small energy gain probably results from the ID-mechanism input to low frequencies, which is balanced by the loss at high frequencies such as shown in Fig. 10d for bin 7, $8f \leq \omega \leq \sqrt{2}8f$. We note that the spectrum $E_7(\rho)$ is steeper than -1.0, but is still a constant-energy-flux spectrum if one considers that $E_1(\rho) \approx \beta^{-0.75}$.

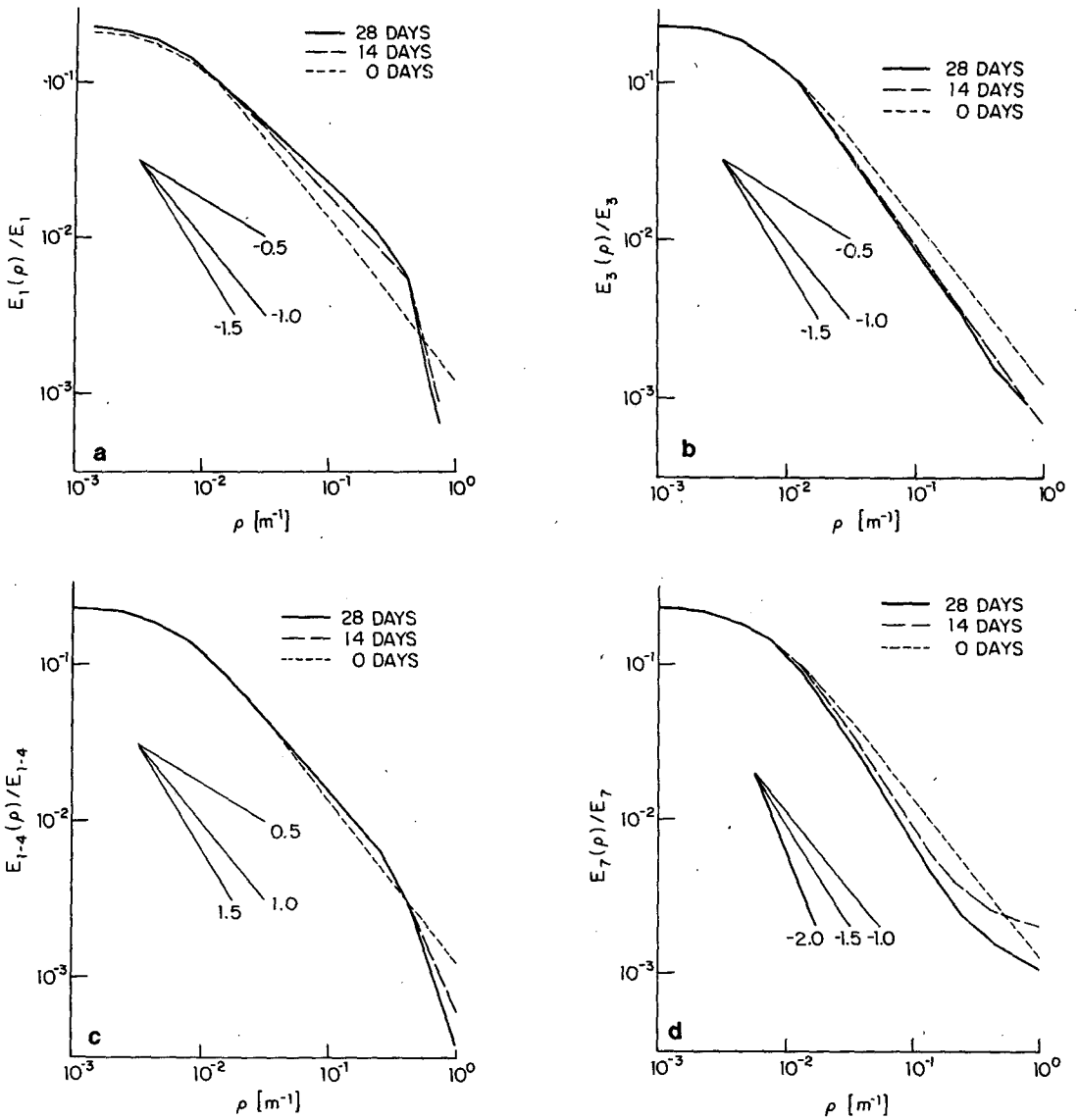

FIG. 10. The evolution of the wavenumber dependence for (a) bin 1, $f \leq \omega \leq \sqrt{2}f$, (b) bin 3, $2f \leq 2\sqrt{2}f$. (c) bins 1–4, $f \leq \omega \leq 4f$, and (d) bin 7, $8f \leq \omega \leq 8\sqrt{2}f$.

Again, the spectrum for the last decade is less steep than for the larger scale waves, which have not had time to equilibrate.

Figs. 11a and 11b show the energy transfer rate by frequency for the wavenumber bins 6 and 8. The figures show a strong transfer into the inertial band $f-2f$ out of $2f-4f$. This transfer decreases with time as an inertial peak is built up. However, the total transfer, denoted on the right-hand side, shows that the transfers nearly cancel out within the band. Fig. 11b shows that bin 8, with shorter time scales, is more nearly compensated at day 28 than the slower evolving bin 6. That is to say, the corrections to the spectrum are working back from the small scales to the slowly evolving large scales in this simulation.

Finally, in Fig. 12 we show the frequency dependence of bin 8. Except for the creation of an inertial peak, the frequency dependence is remarkably stable at a -1.0 slope.

We have attempted to show that in spite of additional details present in the full numerical model, the analytic model quite satisfactorily describes the results. The inertial peak seems to be a necessary dynamic component of the internal-wave spectrum, being built up by the PSI transfer. [Munk and Phillips (1968) showed that the inertial peak might be a horizontal turning point, i.e., kinematic effect, as well.] However, as the peak increases over the body of the spectrum, the transfer rate decreases, suggesting that an equilibrium is possible.

As the spectrum adjusts, creating the inertial peak, the high-frequency small-scale waves with the short time scales equilibrate first, then the corrections work back up the spectrum to the longer-time-scale waves. This implies that changes in the basic characteristics of the internal-wave field, such as changes in slopes, energy levels, fluxes, dissipation time scales, etc., are determined by the slow energy-containing scales, not by the rapidly adjusting small scales. The basic characteristics of the internal-wave field change on the time scale of hundreds of days.

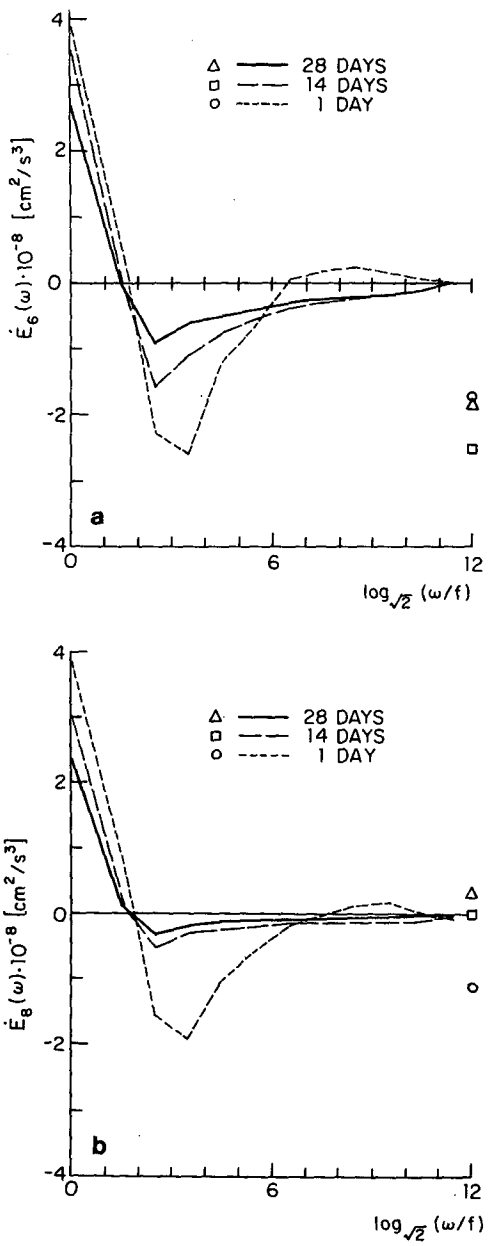

FIG. 11. The evolution of the frequency dependence of the energy transfer rate for (a) bin 6, $10^{-1.75} \leq \rho \leq 10^{-1.5}$ m^{-1} and (b) bin 8, $10^{-1.25} \leq \rho \leq 10^{-1.0}$ m^{-1}. The sum of the transfer rates is shown on the right-hand side. (To convert these values to a uniform transfer rate over the entire range, divide by 12.)

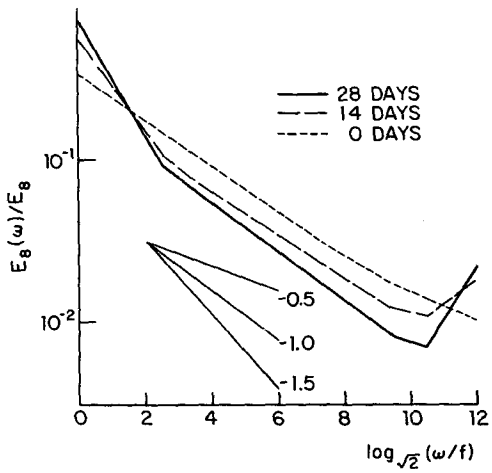

FIG. 12. The evolution of the frequency dependence for bin 8.

7. Difficulties, deficiencies and discussion

We have proposed a model for the dynamic balance of the internal-wave field under the dominating nonlinear transfer mechanisms, the induced diffusion and the parametric-subharmonic-instability mechanism. This balance consists of the following:

1) A stationary vertical-wavenumber spectrum with a constant downscale energy flux under the PSI and ID mechanisms (see Fig. 13). This inertial range with $E(\beta) = E \cdot (\beta/\beta_*)^{-1}$ is not that obtained by the usual dimensional arguments that would conclude $E(\beta) \approx (\beta/\beta_*)^{-2}$ because the dominant mechanisms are nonlocal (in wavenumber space).

2) A downscale flux under the PSI mechanism that is determined by the rate of energy transfer out of the energy-containing scales; this rate determines the overall dissipation rate and the scale at which dissipation becomes important to keep the total shear constant.

3) A downscale flux under the ID mechanism that is determined by matching with the low-frequency region.

4) Both of these fluxes are proportional to the energy times the shear of the large-scale energy-containing waves (so that a 10-fold change in either the energy level or the bandwidth results in a 100-fold change in the energy fluxes and the equivalent viscosity).

5) A spectral model for dissipation, based on a minimum of assumptions, which is smooth, weak and consistent with all of the above points.

This balance reproduces the observed spectral

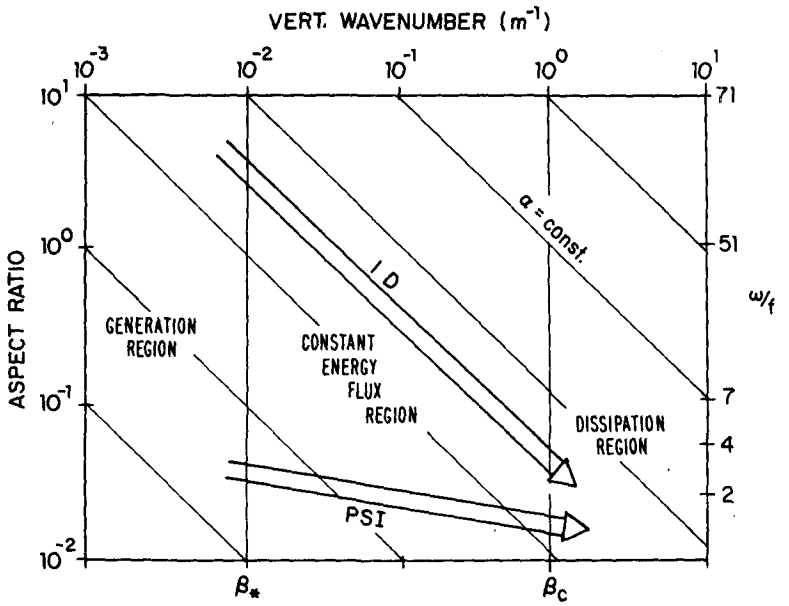

FIG. 13. Schematic representation of the dynamical balance of the internal wave field. Energy is generated at low vertical wavenumbers $\beta < \beta_*$. Between β_* and β_c there is an inertial range where the ID mechanism at high frequencies and the PSI mechanism at low frequencies provide a constant (independent of vertical wavenumber) energy flux to high wavenumbers $\beta > \beta_c$ where energy is dissipated. The break point β_c is determined as the wavenumber where the nonlinear transfer can no longer keep up with dissipation.

slopes and small-scale break point. It is the most complete and consistent model of internal-wave dynamics today. There, however, are several remaining difficulties:

1) There is no explanation for the frequency dependence in the f–$4f$ range. The PSI balance explains the overall vertical-wavenumber dependence, without reliance on the frequency distribution, but there is no information on what the distribution might be. Further, the PSI mechanism removes energy from the $2f$–$4f$ band and transfers it into the f–$2f$ band at smaller scales, building up an inertial peak. As long as there is a downscale flux, this mechanism will deplete the upper frequency band and fill the lower one.

2) Under the ID mechanism the high-frequency region loses energy, which is gained by the near inertial waves. Only in combination is the vertical-wavenumber spectrum stationary. Our high-frequency analytic solution is stationary because it was matched to a stationary low-frequency spectrum. Also, our particular ID solution was selected by matching to the observed low-frequency spectrum. Our balance is hence not completely self-explanatory.

To find the mechanisms which compensate for the frequency transfers we have analyzed the results of a time-stepping numerical model that includes all interacting triads, not just the dominating ones. Although no single mechanisms could be identified, the following points can be conjectured from the model and our analytic results.

The primary effect of the ID mechanism is to make the spectrum smooth by rapid diffusion with the "fast" time scale (MM). The secondary effect is to adjust the spectrum to deliver a constant downscale energy flux in a stationary wavenumber spectrum. This creates a transfer in frequency which is a tertiary effect. At this level, the other interactions become equally important to achieve equilibrium.

The primary result of the PSI mechanism is to create an inertial peak. The secondary effect is to adjust the spectrum to deliver the constant downscale flux. The PSI mechanism, as it creates an inertial peak and depletes the $2f$–$4f$ range, brings itself into partial equilibrium. [$\tau_{\mathrm{PSI}}^{-1} \approx S(2f-4f)$, which is decreasing.] Further the ID mechanism fluxes energy to the depleting PSI region. So partial equilibrium could be achieved by these two mechanisms. For complete equilibrium other (tertiary) not identifiable interactions are required.

The main deficiency of our scenario is that it does not explain the energy and shear level. Both have been observed to be fairly constant. We have found fifty or one hundred days to be the characteristic time scale of the large-scale energy-containing waves. In one hundred days large-scale internal waves travel of the order of 1000 km, a good fraction

of the ocean basin. C. S. Cox and C. L. Johnson and Garrett and Munk (1979) have suggested that this long propagation distance could account for the relatively constant energy level, as sources at many different locations add energy to the internal-wave field, which then spreads out over the basin to achieve a universal level. The internal wave field may be viewed as a massive rotating wheel, spinning constantly with little friction, receiving small, random, hardly noticeable impulses that on average keep it turning at a nearly constant speed (McComas). Or the internal wave field may be viewed as the thermal energy of a nearly insulated large block of highly conducting metal (M. Briscoe). As this block is heated by some randomly distributed Bunsen burners its temperature remains nearly constant. These pictures seem to be likely explanations to us. However, we have shown that the bandwidth is just as important in determining energy fluxes, and its universality is untested.

Similarly, we have offered no explanation why the *root-mean-square* Richardson number $\mathrm{Ri} = N^2/S$ is close to 1. Munk (1981) has suggested that the number of breaking events is extremely sensitive to the rms shear, with $\mathrm{Ri} \approx 1$ a quasi-equilibrium value, so that a slight increase in the shear leads to a large increase in dissipation and a slight decrease leads to essentially no dissipation. This again is a likely explanation. Our balance predicts the spectral slope, width, location and flux of the inertial range, given the overall energy and shear.

Acknowledgments. We would like to thank M. Briscoe for helpful comments and discussions. This work has been supported by the National Science Foundation under Grant OCE77-25803 and by the Office of Naval Research under Contracts N00014-75-C-0225 and N00014-76-C-0197. Computer resources were provided by the Center for Atmospheric Research which is sponsored by the National Science Foundation. This is Contribution No. 4862 from the Woods Hole Oceanographic Institution.

APPENDIX

Details of Numerical Model

The numerical model of Section 6 is a forward-time-stepping model with a fixed time step determined by a multiple of the "slow" time scale for the high-shear waves under the induced diffusion mechanism (MM). That time step is 20 min, or approximately one Väisälä period. Each time step takes 3 s to compute, so a 30-day experiment requires nearly 2 h of Cray time. The 3-seconds computation time is greatly reduced from the 5 min time required by the model previously used by McComas. This time reduction is made possible by the speed, memory, and vector capabilities of the NCAR Cray machine.

The model computes the time rate of change of the internal wave spectrum from the Boltzmann collision integral and the dissipation function.

$$\frac{\partial A}{\partial t}(\mathbf{k}) = \iint d\mathbf{k}'d\mathbf{k}''\{D^+\delta(\mathbf{k}-\mathbf{k}'-\mathbf{k}'')\delta(\omega-\omega'-\omega'') \times [A(\mathbf{k}')A(\mathbf{k}'') - A(\mathbf{k})A(\mathbf{k}') - A(\mathbf{k})A(\mathbf{k}')] + 2D^-\delta(\mathbf{k}-\mathbf{k}'+\mathbf{k}'')\delta(\omega-\omega'+\omega'') \times [A(\mathbf{k}')A(\mathbf{k}'') + A(\mathbf{k})A(\mathbf{k}') - A(\mathbf{k})A(\mathbf{k}'')]\} - \nu\omega^{-1}S(\mathbf{k}), \quad \text{(A1)}$$

where ν is the effective viscosity.

This prescription is manipulated to use finite elements, matrix equations, energy conservation and machine vectorization. The spectrum is represented in terms of finite elements in logarithmic space, i.e.,

$$A(\omega, \rho) = \exp[\sum_j a_j\phi_j(\omega, \rho)], \quad \text{(A2)}$$

where $\phi_j(\omega, \rho)$ is a bilinear interpolator in logarithmic space $\log_{\sqrt{2}}\omega$, $\log_{10}\rho$. This allows a simple interpolation routine, with only minor restrictions on the power law dependency of $A(\omega, \rho)$. Eq. (A1) is then multiplied by $\omega\phi_i$ and integrated over all $\mathbf{k}$ to yield

$$B_{ij}\dot{a}_j = c_i + d_i. \quad \text{(A3)}$$

Here

$$B_{ij} = \int E(\mathbf{k})\phi_i(\mathbf{k})\phi_j(\mathbf{k})d\mathbf{k} \quad \text{(A4)}$$

denotes the energy matrix such that $\sum_j B_{ij}$ is the energy in ϕ_i and $\sum_i \sum_j B_{ij}$ the total energy. The vector

$$c_i = \iiint d\mathbf{k}'d\mathbf{k}''d\mathbf{k}D^+\delta(\mathbf{k}-\mathbf{k}'-\mathbf{k}'')\delta(\omega-\omega'-\omega'') \times [\omega\phi_i(\mathbf{k}) - \omega'\phi_i(\mathbf{k}') - \omega''\phi_i(\mathbf{k}'')] \times \{A(\mathbf{k}')A(\mathbf{k}'') - A(\mathbf{k})A(\mathbf{k}') - A(\mathbf{k})A(\mathbf{k}'')\} \quad \text{(A5)}$$

describes the energy change in ϕ_i, with $\sum_i c_i = 0$ because of energy conservation. [Since $\sum_i \phi_i(\mathbf{k}) = 1$ the term in brackets is zero because of the frequency resonance condition.]

The energy matrix B_{ij} and c_i must be computed at every time step, a time consuming task. The B_{ij} are computed in terms of exponential integrals. The c_i's are computed on a grid nested within the 13 × 13 grid defining the a's and ϕ's (See Fig. 14). The model steps along this interior 25 × 25 grid, computing the interactions of 121 triads that interact with the wave at that point. The energy transferred at each triad member is summed to the appropriate c_i, the next triad is chosen, etc., the next grid point is chosen, etc., until all 75 625 triads are computed.

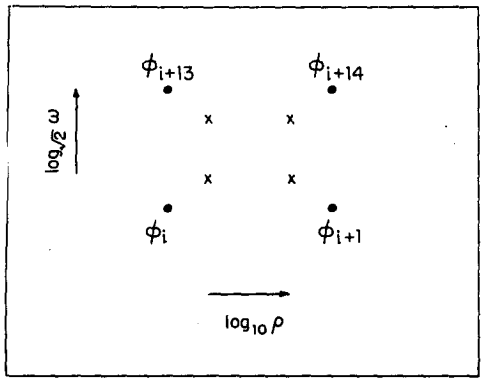

FIG. 14. Numerical grid for the spectrum (dots) and for the interaction calculation (crosses).

The dissipation is computed as

$$d_i = -\nu S_i, \tag{A6}$$

where

$$S_i = \int S(\mathbf{k})\phi_i(\mathbf{k})d\mathbf{k} \tag{A7}$$

is the shear vector such that S_i is the shear in ϕ_i, and $\sum_i S_i$ is the total shear. The shear vector S_i also must be computed at every time step.

Finally, the $\dot{a}$'s are computed from the banded matrix problem (A3), and the new amplitudes found by forward-time stepping.

$$a_{t+\Delta t} = a_t + \dot{a}_{t+\Delta t}\Delta t. \tag{A8}$$

The whole process repeats for the next time step.

REFERENCES

Bell, T. H., 1975: Topographically generated internal waves in the open ocean. *J. Geophys. Res.*, **80**, 320–327.

——, 1978: Radiation damping of inertial oscillations in the upper ocean. *J. Fluid Mech.*, **88**, 289–308.

Cairns, J. L., and G. O. Williams, 1976: Internal wave observations from a midwater float, 2. *J. Geophys Res.*, **81**, 1943–1950.

Gargett, A. E., T. J. Hendricks, T. B. Sanford, T. R. Osborne, and A. J. Williams, III, 1981: A composite spectrum of vertical shear in the upper ocean. *J. Phys. Oceanogr.*, **11** (in press).

Garrett, C. J. R., 1979: Mixing in the ocean interior. *Dyn. Atmos. Oceans*, **3**, 239–265.

——, and W. H. Munk, 1972a: Space-time scales of internal waves. *Geophys. Fluid Dyn.*, **2**, 225–264.

——, and ——, 1972b: Oceanic mixing by breaking internal waves. *Deep-Sea Res.*, **19**, 823–832.

——, and ——, 1975: Space-time scales of internal waves: A progress report. *J. Geophys. Res.*, **80**, 291–297.

——, and ——, 1979: Internal waves in the ocean. *Annual Review of Fluid Mechanics*, Vol. 11, Annual Reviews, Inc. 339–369.

Gregg, M. C., 1977: Variations in the intensity of small-scale mixing in the main thermocline. *J. Phys. Oceanogr.*, **7**, 436–454.

Hasselmann, K., 1974: On the spectral dissipation of ocean waves due to white capping. *Bound-Layer Meteor.*, **6**, 107–127.

Holloway, G., 1980: Oceanic internal waves are not weak waves. *J. Phys. Oceanogr.*, **10**, 906–914.

Käse, R. H., 1979. Calculations of the energy transfer by the wind to near-inertial internal waves. *Deep-Sea Res.*, **26**, 227–232.

Leaman, K. D., and T. B. Sanford, 1975: Vertical energy propagation of inertial waves: A vector spectral analysis of velocity profiles. *J. Geophys. Res.*, **80**, 1975–1978.

McComas, C. H., 1977: Equilibrium mechanisms within the oceanic internal wave field. *J. Phys. Oceanogr.*, **7**, 836–845.

McComas, C. H., and F. P. Bretherton, 1977: Resonant interaction of oceanic internal waves. *J. Geophys. Res.*, **82**, 1397–1412.

——, and M. G. Briscoe, 1980: Bispectra of internal waves. *J. Fluid Mech.*, **97**, 205–213.

McComas, C. H., and P. Müller, 1981. Time scales of resonant interactions among oceanic internal waves. *J. Phys. Oceanogr.*, **11**, 139–147.

Müller, P., 1977: Spectral features of the energy transfer between internal waves and a larger scale shear flow. *Dyn. Atmos. Oceans*, **2**, 49–72.

——, and D. J. Olbers, 1975: On the dynamics of internal waves in the ocean. *J. Geophys. Res.*, **80**, 3848–3860.

——, ——, and J. Willebrand, 1978: The IWEX spectrum. *J. Geophys. Res.*, **83**, 479–500.

Munk, W. H., 1981: Internal waves and small scale processes. *Evolution of Physical Oceanography*, B. A. Warren and C. Wunsch, Eds., The MIT Press, 264–291.

——, and N. Phillips, 1968: Coherence and band structure of inertial motion in the sea. *Rev. Geophys.*, **6**, 447–472.

Olbers, D. J., 1976: Nonlinear energy transfer and the energy balance of the internal wave field in the deep ocean. *J. Fluid Mech.*, **74**, 375–399.

Orlanski, I., and K. Bryan, 1969: Formation of the thermocline step structure of large-amplitude internal gravity waves. *J. Geophys. Res.*, **74**, 6975–6983.

——, and C. P. Cerasoli, 1980: Resonant and non-resonant wave-wave interactions for internal gravity waves. *Marine Turbulence*, J. Nihoul Ed., Elsevier, 65–100.